International Journal of Adhesion & Adhesives 33 (2012) 61–66

Contents lists available at SciVerse ScienceDirect

International Journal of Adhesion & Adhesives

journal homepage: www.elsevier.com/locate/ijadhadh

Characterization of nano scale adhesion at solid surface of oxidized PP wax/PP blends

Ali Salimi *

Faculty of Polymer Processing, Iran Polymer and Petrochemical Institute (IPPI), P. O. Box 14965/115, Tehran, Iran

ARTICLE INFO

Article history:
Accepted 8 November 2011
Available online 25 November 2011

Keywords:
Work of adhesion
Atomic force microscopy
Surface roughness
Polyolefins
JKR approximation

ABSTRACT

The incorporation of oxidized PP wax OPPW additive into polypropylene resulted to the improved surface adhesion. Atomic force microscopy (AFM) was employed to show either the surface topography or the changes in adhesion force measurements between the probe tip and sample surface. The results of surface characterization tests revealed lower surface roughness and higher adhesion force for higher OPPW content in the blends. The lower surface roughness may be attributed to higher melt flow ability of OPPW and hence better mold filling during sample fabrication. The improvement of surface adhesion was in favor for wetting behavior of solid surface using three test liquids of distilled water, diiodomethane and formamide. The thermodynamic work of adhesion W_a was calculated from surface free energy components using geometric mean model of Owens–Wendt–Rabel and Kaelble (OWRK approach) and also from the theory of van Oss–Good–Chaudhary (VOGC approach). The adhesion force measurements in AFM were also employed to derive the W_a using Johnson–Kendal–Roberts (JKR approximation). The results indicate that the increase in W_a was mainly due to polar part in OWRK approach and the acid–base part in VOGC approach. However, the results of work of adhesion in JKR approximation does not in general scale linearly with the respective OPPW content for the sample series, may be due to varying in near-surface modulus. The adhesion promoting effect of OPPW in the blends seems to work mainly via increasing surface acid–base interactions, better surface wettability and to some extent by plastic deformation mechanisms during debonding.

1. Introduction

Due to chemical inertness and absence of polar groups at the near-surface region, polypropylene (PP) suffers the lack of good surface adhesion. Several surface modification methods for polyolefins have been introduced in applications such as bonding, coating and biocompatibility to solve the problem of low surface adhesion [1–3]. The incorporation of polar additives into polymer matrix may be considered as an effective approach in improving surface adhesion [3,4]. However, some drawbacks such as chemical incompatibility between ingredients maybe involved in polymer structure in which affects the mechanical properties of the blends, adversely [3–5].

The thermodynamic work of adhesion W_a may be considered as supporting factor for adhesion enhancement mechanisms. The practical adhesion measurements mainly reflect the mechanical response of the interface in combination with the theoretical W_a [6,7]. Among different approaches for calculation of thermodynamic W_a, the use of surface tension components and also such components for solid surfaces showed reliable results in adsorption theory of adhesion [7–9]. Based on the geometric mean model proposed by Owens–Wendt–Rabel and Kaelble (OWRK approach), the dispersive and polar components of solid surface free energy and also those of liquid phase combine together to measure the interfacial thermodynamic W_a between two phases [1,7–9]. The interfacial thermodynamic W_a can be also obtained in acid–base theory as proposed by van Oss, Good and Chaudhary (VOGC approach). It was suggested that the acidity (electron acceptor) and basicity (electron donor) properties of the surface could be related more closely to the chemical nature of the phases [9,10]. Several papers have tried to demonstrate the correlation between the measured adhesion strength and the surface free energy to the interfacial W_a [7,11,12]. It was shown that the interfacial W_a mainly correlates well to the surface forces acting between various substrates. However, some wood/coating systems show the lack of good correlation between the interfacial W_a and the measured strength of adhesion [7].

Recently, some newer surface characterization techniques of atomic force microscopy (AFM) were developed for measuring the sample surface force in nanometer-scale. Numerous techniques and surface force apparatus have been introduced as variations of the original contact mode design such as using organic liquids for

* Tel.: +98 21 44580000, +98 21 44580019; fax: +98 21 44580021.
E-mail address: a.salimi@ippi.ac.ir

0143-7496/$ - see front matter © 2011 Elsevier Ltd. All rights reserved.
doi:10.1016/j.ijadhadh.2011.11.004

studying the chemical interactions at the interface [13–16]. The polymer-coated tip or particle of ink was also used to measure the adhesion force between two solid phases [17]. The torsional harmonic AFM technique was successfully used in mapping the adhesion force of pigment latex coated paper sample yielding a good correlation between W_a and surface energy values [18]. The data of surface force may be then used in different theories of contact mechanics to give a measure of W_a [19,20]. Based on the well-defined approach proposed by Johnson–Kendal–Roberts (JKR approximation), the pull-off force is related directly to the W_a for most polymer systems [13,15,16,19,20]. The requirements of a soft contact mechanics was provided by the results of nano-indentation test in the previous work [21]. However, the limitation of this testing method including the sample compliance and transparency to detect the contact area has to be considered [13,19].

In this study, the adhesion force at solid surface of modified PP is to be evaluated using distance dependent measurement DDM technique in contact mode AFM. The contact angle measurements provide the surface wettability data and an indirect measure of thermodynamic W_a using two well-defined approaches in adsorption theory of adhesion. The comparison between the thermodynamic W_a and direct adhesion measurements in AFM help us to get better insights into the adhesion enhancement mechanisms of OPPW.

2. Experimental

2.1. Materials

The oxidized PP wax OPPW as polar additive was added into PP homopolymer in 2, 6 and 10 wt% content, namely C2, C6 and C10, respectively. The OPPW with acid value of 13.5 mg KOH/g was prepared according to the procedure reported elsewhere [4]. The blending was conducted in a Haake SYS 90 (USA) internal mixer at 190 °C for 10 min. The melt flow index *MFI* of each OPPW/PP blend was measured in Zwick 4100 (Germany). The procedure was in accordance to ISO 1133-03 at 230 °C using a weight of 2.16 kg. The sample sheet ($32 \times 20 \times 2$ mm^3) of each blend was then fabricated by injection molding in a minimolder, Dynisco polymer test (USA) at 210 °C. The sample sheets of each OPPW/PP blend were then used in surface characterization tests including surface topography, adhesion force measurements and surface wettability.

2.2. Surface characterization

A commercial AFM, Dualscope/Rasterscope C26, DME (Denmark) was used in this study. Both non-contact and contact modes of AFM were employed to show the surface topography changes and adhesion force measurements, respectively. In both techniques, a stiff silicon nitride cantilever with a spring constant of about 28 N/m and tip apex radius of ~10 nm was used. After capturing the surface images, the roughness parameter R_a and R_q were determined using arithmetic average of values of surface heights and the root mean square RMS deviation from surface heights, respectively. Roughness values were recorded in AC probe scanning area of 500×500 nm^2.

The technique of DDM was used for the adhesion force measurements. The measurements were conducted at various locations on sample sheet and five times per each point. The speed of the DC probe tip movement was 1000 nm/s. The recorded force–distance curves were then used to quantitatively measure the adhesion force by performing a calibration of force constant of the cantilever. The adhesion force is measured as the pull-off distance at which cantilever retracts from the surface to a position in which there is no net force between the tip and sample surface.

The surface wettability of the blends was determined through the static contact angle measurements of the three test liquids. The test liquids of distilled water, formamide and diiodo methane were tested in a Krüss G2/G40 (Germany) contact angle measuring system. Each test liquid (5 μL) was dispensed onto sample surface for five times and the average values with standard deviations were reported. The resulting contact angles were then used for calculating the components of surface free energy of solid phase and the interfacial W_a between various OPPW/PP blends and liquid phase.

2.3. Calculations of the work of adhesion

The interfacial W_a was calculated via combining the components of surface tension of the probe liquids and also such components for solid surfaces. The combination of the respective components was conducted based on OWRK approach and also VOGC approach. Table 1 shows the total surface tension γ^{tot} and its components for the probe test liquids.

Where γ^A, γ^B, γ^{AB} and γ^{LW} refer to acidic, basic, acid–base and Lifshitz–van der Waals components of the probe liquid, respectively (VOGC approach). The γ^P and γ^d are the polar and dispersive components of the probe liquid, respectively (OWRK approach). In OWRK approach, the contact angle data of at least two different liquids are needed to calculate two unknown surface free energy components, i.e., the polar component γ_S^P and the dispersive component γ_S^d of the solid surface free energy. After Dupré equation of W_a, the interfacial W_a between two condensed phases may be simplified as a combination of its polar and dispersive parts, i.e. W_a^P and W_a^D, respectively, and can be calculated according to Eqs. (1)–(3) [1,8,13]

$$W_a = {W_a}^P + {W_a}^D \tag{1}$$

$${W_a}^P = 2\sqrt{{\gamma_S}^P {\gamma_L}^P} \tag{2}$$

$${W_a}^D = 2\sqrt{{\gamma_S}^d {\gamma_L}^d} \tag{3}$$

In OWRK approach, only two probe liquids (distilled water and diiodomethane) were used to calculate the W_a.

In VOGC approach, the contact angle data for at least three different liquids are needed to calculate three unknown surface components, i.e., the acidic component γ_S^A, the basic γ_S^B and the Lifshitz–van der Waals component γ_S^{LW} of the solid surface free energy. In VOGC approach, the interfacial W_a is a combination of

Table 1
Total surface tension γ^{tot} and its components of probe test liquids at 20 °C [9].

Probe liquid	γ^B (dyn/cm)	γ^A (dyn/cm)	γ^{AB} (dyn/cm)	γ^{LW} (dyn/cm)	γ^d (dyn/cm)	γ^P dyn/cm)	γ^{tot} (dyn/cm)
Distilled water	25.5	25.5	51	21.8	21.8	51	72.8
Diiodo methane	0	~0	0	50.8	50.8	0	50.8
Formamide	39.6	2.28	19	39.2	39.5	18.7	56

its Lifshitz–van der Waals and acid–base parts, i.e., W_a^{LW} and W_a^{AB}, respectively, and can be then calculated using simplified Eqs. (4)–(6) [1,8]

$$W_a = W_a{}^{LW} + W_a{}^{AB} \tag{4}$$

$$W_a{}^{LW} = 2\sqrt{\gamma_S{}^{LW}\gamma_L{}^{LW}} \tag{5}$$

$$W_a{}^{AB} = 2\sqrt{\gamma_S{}^{A}\gamma_L{}^{B}} + 2\sqrt{\gamma_S{}^{B}\gamma_L{}^{A}} \tag{6}$$

In VOGC approach, all probe liquids (Table 1) were utilized to calculate the W_a.

3. Results and discussion

3.1. Studies of surface topography and adhesion forces

Fig. 1 shows the non-contact AFM topographic images of the neat PP and its blends with OPPW, i.e., sample C2, C6 and C10.

As shown in Fig. 1a, the surface of neat PP sample is characterized by a fiber-like structure. The parallel strands on sample surface seem to be due to the orientation of melt flows. Due to the temperature difference between polymer melt and the mold surface, the melt was stretched and holes are formed on sample surface during mold filling. The holes were also oriented along the direction of melt injection resulting to formation of parallel strands on sample surface. In comparison with neat PP sample, it is clear that the surface coarseness decreases in Fig. 1b–d.

The measurements of roughness values based on the arithmetic average of surface heights R_a and the RMS roughness R_q were tabulated in Table 2.

As shown in Table 2, there seems to be a tendency for decreased surface roughness for the samples with higher OPPW content. This phenomenon is probably attributed to the lubricating effect of OPPW which means that the polymer melt runs more easily as the OPPW content increases. In comparison with neat PP macromolecules, the OPPW has shorter chains hence providing more melt flow ability for PP chains [4]. As clearly mentioned in the preparation process, the lower molecular weight of OPPW was due to the chain scission in thermo-oxidation process [4]. These findings are in agreement with the results of *MFI*. The higher *MFI* indicates higher melt flow and lower melt viscosity. The neat PP has *MFI*= 8 g/10 min whereas the *MFI* of the blends showed substantial increase. It increased to 28 g/10 min by incorporation of 2 wt% OPPW (sample C2) and 32 g/10 min for sample C10. It means that even small amount of OPPW has great impact on the melt flow ability of the blends. The higher flow ability in PP containing OPPW may result to better mold filling during injection molding and hence less probable formation of the holes and grooves on the surface. The decreasing trend for surface roughness has been revealed before in AFM topography images in Fig. 1a–d.

At next step, the DDM technique in contact mode AFM was employed to probe the adhesion force between the tip and polymer surface. Fig. 2 illustrates a typical distance-dependent curve showing both the approach and withdrawal curves for a Si tip interaction with solid surface of PP/OPPW blend.

Table 2
Surface roughness values of neat PP, C2, C6 and C10.

Sample	Neat PP	C2	C6	C10
R_a (nm)	9.2	5.2	4.3	4.9
R_q (nm)	11.5	6.5	5.9	6.2

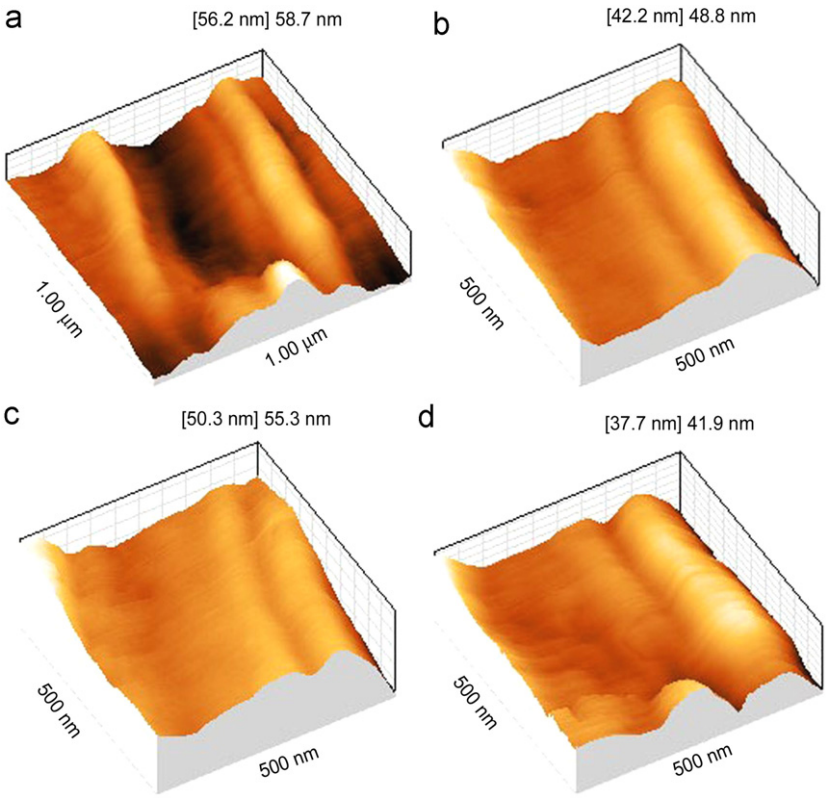

Fig. 1. AFM pictures of (a) neat PP, (b) C2, (c) C6 and (d) C10.

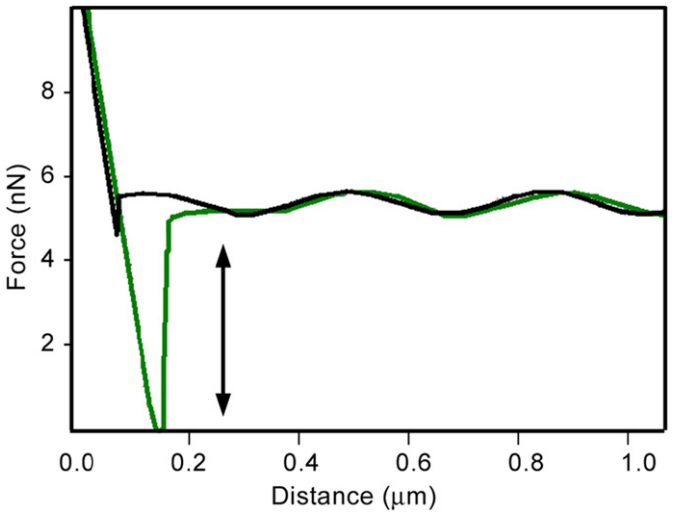

Fig. 2. The typical distance dependent curve showing the approach curve (darker line) and the withdrawal curve (lighter line) for Si tip interaction with solid surface of OPPW/PP blend. The arrow shows the amount of adhesion force.

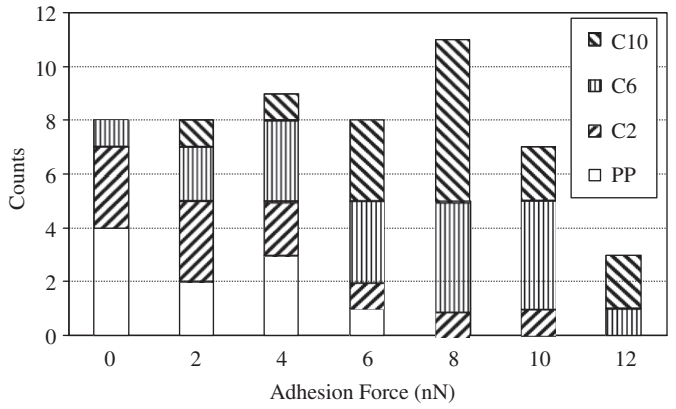

Fig. 3. Histograms of adhesion force for neat PP, C2, C6 and C10.

The force–distance curves were measured by bringing the tip from a distance (e.g. 1000 nm) to make contact between the tip and sample surface followed by the retraction of the tip from the surface. The amount of retraction shows the level of adhesion force between the tip and the solid surface at the point where the tip is pulled from the surface. That was clearly indicated by an arrow and yields the adhesion force of ~4.8 nN for the data in Fig. 2.

The distribution of the adhesion force for neat PP and its blends with OPPW, i.e., C2, C6 and C 10 are shown in histograms in Fig. 3.

As shown in Fig. 3, the adhesion forces are shown in a set of round numbers. However, the deviation in adhesion force for each sample was considered in the calculation of W_a as error bars. The histogram of adhesion force may be well considered as an examination of the reproducibility of the changes in adhesion force. A degree of distribution in the adhesion force can be seen for each sample in Fig. 3. However, the number of counts in each set of adhesion force determines the trend of surface adhesion for each sample. For example, in neat PP the number of counts at zero force is four of eight, accounting for the half of the total counts in zero adhesion force. Therefore, the much number of counts at low adhesion force accounts mainly for lower surface adhesion. In Fig. 3 it may be concluded that the number of counts in high adhesion forces increased as the OPPW content increased in the PP/OPPW blends. Besides, the total number of counts for the range of adhesion force between 0 nN to 12 nN was the highest for the sample C6 and C10 and recorded to 18 and 15, respectively.

Using the total number of counts for the range of adhesion force between 0 nN to 12 nN, the average value of adhesion force was calculated as 2.2 nN with standard deviation (STD 0.9) for neat PP and increases to 3.5 nN (STD 1.7), 6.6 nN (STD 1.2) and 8.1 nN (STD 2.1) for C2, C6 and C10, respectively. It may be concluded that the average value for adhesion force measurement indicates an increase by the OPPW content of the blends. Besides, the total counts of adhesion force get scattered for the neat PP and sample C2. The interpretation in force–distance curves may be related to the lack of exact calibration of spring constant of cantilever. Even the presence of surface contaminations or the degree of surface coarseness at the point of contact may be considered as one main reason to bring about widely scattering data in adhesion forces [16]. It is likely that the surface roughness in PP and C2 are responsible for this broad distribution of adhesion forces. In force–displacement measurements and in retraction approach, the molecular reconstruction experienced by the near-surface molecules may also give the reason for deviation from JKR approximation [18,20]. The average value of adhesion force was then used in contact mechanics for measuring the W_a and will be presented in Section 3.3 together with the possible mechanisms in improving adhesion in OPPW/PP blends

3.2. Study of surface wettability

The contact angles of three probe liquids on sample surface of the neat PP, C2, C6 and C10 are shown in Fig. 4.

As shown in Fig. 4, there is declining trend for contact angle of all probe liquids. However, the trend is more pronounced for water drop which is a polar liquid. Smaller contact angle indicates more wetting property of the surface and higher surface free energy [6,8]. Diiodomethane did not show any considerable changes and the contact angle remained at around 52° may be due to its non-polar nature. In a survey on chemical composition of surface, an increase in various oxygen-based functionalities such as carbonyl and hydroxyl groups was observed using ATR-FTIR technique [4]. The introduction of polar OPPW in the blends results to increasing population of polar groups and hence better attraction to polar liquids, i.e., better surface wettability.

The results of contact angle in each sample and the respective components of probe liquid surface tension (Table 1) were then utilized to find the solid sample surface free energy and its respective components. The surface free energies of solid sample were further employed for the calculation of interfacial W_a in

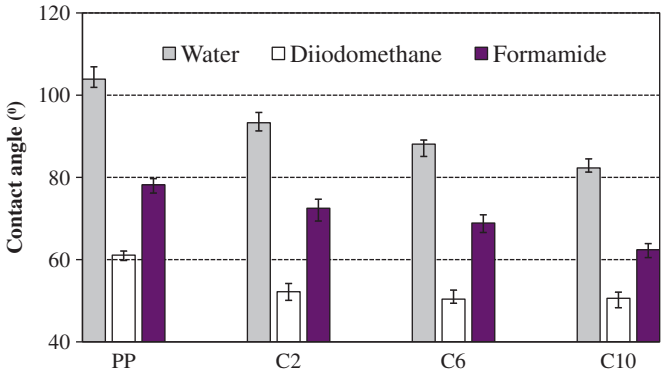

Fig. 4. Contact angles of water, diiodomethane and formamide for the neat PP, C2, C6 and C10.

Section 3.3 together with the possible mechanisms in improving adhesion in adhesion adsorption theory.

3.3. Calculations of the work of adhesion

The average value of adhesion force may be used in contact mechanics for measuring the W_a. Based on the simple JKR approximation for a tip radius of R, the adhesion force F is related directly to the W_a according to Eq. (7) [15,20]

$$F = -1.5\pi R W_a \quad (7)$$

For a regular tip of $R=10$ nm, a relatively well-defined interface with the sample surface is formed providing a rather ideal measuring of possible bond strength. Hence, the change in F is then a measure of W_a or the interfacial energy between the tip and sample surface. For this reason the average adhesion forces of up to $F=$ 8 nN in nano-scale force–displacement curves, would translate into a reasonable W_a value of about 170 mJ/m^2.

According to Eqs. (1)–(3) and Eqs. (4)–(6), it is possible to measure the W_a using respective surface free energy components in two well-defined approaches, i.e., OWRK and VOGC approaches in adsorption theory of adhesion. The calculations of solid surface free energies were conducted by the software supplied by Krüss for both OWRK and VOGC approaches. Then the thermodynamic W_a and its respective parts were derived using Eqs. (1)–(3) (OWRK approach) and Eqs. (4)–(6) (VOGC approach). Note that the thermodynamic W_a may be calculated between a couple of phases, i.e., solid surface of each blend and each of the probe liquids. Here, only the data of W_a between water and solid surface of each blend OPPW/PP was reported. The contribution of each part of W_a were shown in OWRK and VOGC approaches in Figs. 5 and 6, respectively.

As shown in both Figs. 5 and 6, there are similar rising trend by the increase in OPPW content. In Fig. 5, the contribution of the W_a^D was ever higher than the W_a^P. The W_a^P showed pronounced changes on OPPW content which indicates the stronger effect of polar interactions at the interface in comparison with dispersive forces. In both Figs. 5 and 6 the error bars refer to the variations in contact angle measurements.

As shown in Fig. 6, the contribution of W_a^{AB} was getting higher for the higher OPPW content. It was seen that about 39% of the total W_a was due to the acid–base interactions in sample C10. The incorporation of OPPW results to good surface wetting properties and reveals highly polar groups on the sample surface and hence increase the electron donor (acidity) and electron acceptor (basicity) properties of surface. Regardless of the lowering roughness, the adhesion promoting effect of OPPW in the blends seems to work mainly via increasing surface acid–base interactions and also better surface wettability.

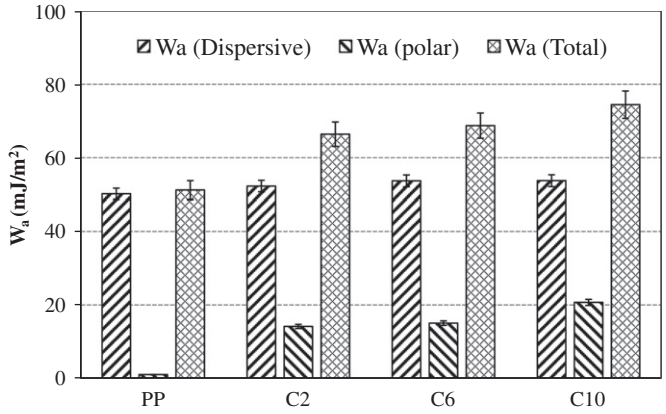

Fig. 5. Contribution of dispersive (W_a^D) and polar part (W_a^P) of the interfacial W_a in OWRK approach. The interfacial W_a was calculated for interface between solid surface of each blend and water.

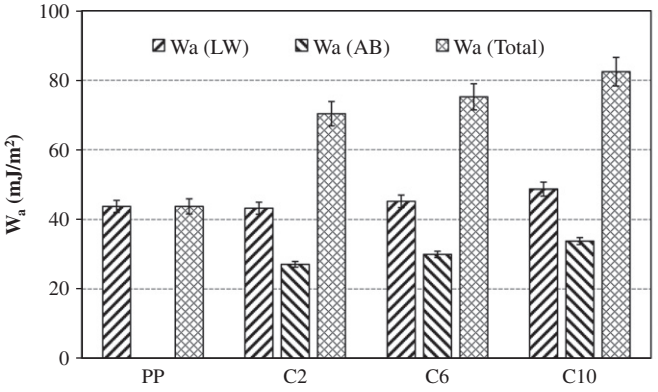

Fig. 6. contribution of Lifshitz–van der Waals part (W_a^{LW}) and acid–base part (W_a^{AB}) of the interfacial W_a in VOGC approach. The interfacial W_a was calculated for interface between solid surface of each blend and water.

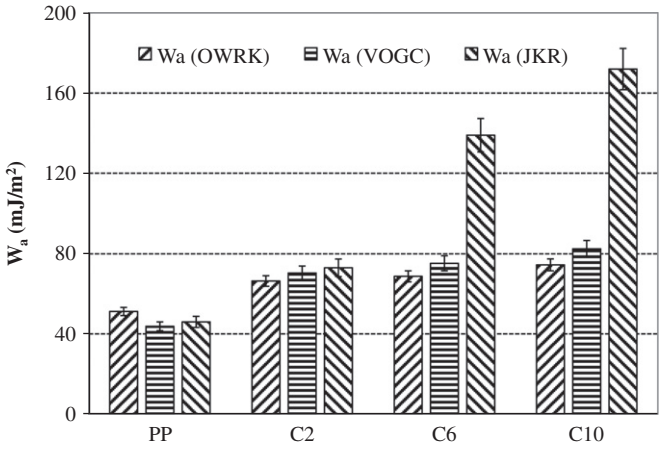

Fig. 7. trend of W_a values based on the OWRK approach, VOGC approach and JKR approximation.

The trend of thermodynamic W_a in each approach and the measured W_a value in JKR approximation was shown in Fig. 7.

As shown in Fig. 7, the W_a obtained by two approaches give satisfactory results in comparison with the JKR based W_a obtained from nano-sale adhesion tests. The W_a based on the VOGC approach seems to have a better agreement to the W_a value in JKR approximation. The theory behind the surface free energy approaches stands on the physics of molecular attractions while that of JKR approach accounts for the mechanical contact deformation [18,20]. In JKR contact mechanics, the intense increase in W_a in samples of high OPPW content, i.e., C6 and C10 may originates from the energy dissipation phenomenon at the interface. The changes in modulus substrate at the near-surface region of sample sheets were studied by nano indentation tests, elsewhere [21]. For high OPPW content, the lower modulus at near-surface of the sample sheets provides higher plastic deformation during tip retraction and hence higher W_a recorded. In other words, the lower near-surface modulus may involve to some extent to the adhesion enhancement mechanisms [22]. In brief the changes in total W_a in JKR approach corresponds to the changes both in thermodynamic W_a and work of plastic deformation during adhesion test.

4. Conclusion

The surface topography images revealed a decrease in surface roughness as a result of incorporation of OPPW. The lower value

for surface roughness was mainly due to the higher flow ability in PP containing OPPW. The OPPW are short chains providing lubricating effect during mold filling.

In nano scale adhesion measurements, the DDM technique yielded an increase in average surface adhesion forces as the OPPW content increases. Besides, the data scattering may be due to the effect of surface roughness on exact determination of tip-sample loading. Analysis of force spectroscopy yielded adhesion forces up to 12 nN translating a W_a of about 255 mJ/m^2. The results indicate that the W_a from both thermodynamic approaches and the surface wetting properties were more or less dependent on OPPW concentration. The W_a^P and W_a^{AB} showed pronounced effects on the total W_a value so that about 39% of W_a was due to the acid-base interactions in sample C10. The W_a calculated via the surface free energy components in VOGC approach shows better agreement with the adhesion measurements from JKR approximation from contact mechanics. The results of W_a in JKR model does not in general scale linearly with the respective OPPW content for the sample series maybe due to the varying in near-surface modulus.

Regardless of the lowering roughness, the adhesion promoting effect of OPPW in the blends seems to work mainly via increasing the surface acid–base interactions and also better surface wettability and to some extent by plastic deformation mechanisms during debonding.

Acknowledgement

The author thanks Dr P. Marashi from Maharfan Abzar Co (Tehran, Iran) for the support with the AFM system and also Miss A. Tatlari from IPPI in reproducing figures.

References

[1] Awaja F, Gilbert M, Kelly G, Fox B, Pigram PJ. Adhesion of polymers. Prog Polym Sci 2009;34:948–68.
[2] Jaehnichen K, Frank J, Pleul D, Simon F. Study of paint adhesion to polymeric substrates. J Adhes Sci Technol 2003;17:1635–54.
[3] Noeske M, Degenhardt J, Strudthoff S, Lommatzsch U. Plasma jet treatment of five polymers at atmospheric pressure: surface modifications and the relevance for adhesion. Int J Adhes Adhes 2004;24:171–7.
[4] Salimi A, Mirabedini M, Atai M, Mohseni M. Studies on the mechanical properties and practical coating adhesion on PP modified by oxidized wax. J Adhes Sci Technol 2010;24:1113–29.
[5] Novak I, Krupa I, Luyt AS. Modification of the polarity and adhesive properties of polyolefins through blending with maleic anhydride grafted Fischer–Tropsch paraffin wax. J Appl Polym Sci 2006;100:3069–74.
[6] Packham DE. Surface energy, surface topography and adhesion. Int J Adhes Adhes 2003;23:437–48.
[7] Clint JH. Adhesion and components of solid surface energies. Curr Opin Colloid Interface Sci 2001;6:28–33.
[8] Fourche G. An overview of the basic aspects of polymer adhesion part 1: fundamentals. Polym Eng Sci 1995;35:957–67.
[9] Gindl M, Sinn G, Gindl W, Reiterer A, Tschegg SA. Comparison of different methods to calculate the surface free energy of wood using contact angle measurements. Colloids Surf A 2001;181:279–87.
[10] Van Oss CJ. Use of the combined Lifshitz–van der Waals and Lewis acid–base approaches in determining the apolar and polar contributions to surface and interfacial tensions and free energies. J Adhes Sci Technol 2002;16:669–77.
[11] Clear SC, Nealey PF. Chemical force microscopy study of adhesion and friction between surfaces functionalized with self-assembled monolayers and immersed in solvents. J. Colloid Interface Sci 1999;213:238–50.
[12] Wolkenhauer A, Avramidis G, Hauswald E, Militz H, Viöl W. Sanding vs. plasma treatment of aged wood: a comparison with respect to surface energy. Int J Adhes Adhes 2009;29:18–22.
[13] Oláh A, Vancso GJ. Characterization of adhesion at solid surfaces: development of an adhesion-testing device. Euro Polym J 2005;41:2803–23.
[14] Leite F, Herrmann P. Application of atomic force spectroscopy (AFS) to studies of adhesion phenomena. J Adhes Sci Technol 2005;19:365–405.
[15] Nie HY, Walzak MJ, Berno B, McIntyre NS. Atomic force microscopy study of polypropylene surfaces treated by UV and ozone exposure: modification of morphology and adhesion force. Appl Surf Sci 1999;144–145:627–32.
[16] Thio BJR, Meredith JC. Measurement of polyamide and polystyrene adhesion with coated-tip atomic force microscopy. J Colloid Interface Sci 2007;314:52–62.
[17] Segeren LHGJ, Siebum B, Karssenberg FG, Van Den Berg JWA, Vancso GJ. Micro particle adhesion studies by atomic force microscopy. J Adhes Sci Technol 2002;16:793–828.
[18] Ihalainen P, Järnström J, Määttänen A, Peltonen J. Nano-scale mapping of mechanical and chemical surface properties of pigment coated surfaces by torsional harmonic atomic force microscopy. Colloids Surf A 2011;373:138–44.
[19] Wu K-C, You H-I. Determination of solid material elastic modulus and surface energy based on JKR contact model. Appl Surf Sci 2007;253:8530–7.
[20] Grierson DS, Flater EE, Carpick RW. Accounting for the JKR-DMT transition in adhesion and friction measurements with atomic force microscopy. J Adhes Sci Technol 2005;19:291–311.
[21] Salimi A, Mirabedini SM, Atai M, Mohseni M, Naimi-Jamal MR. Correlating the adhesion of an acrylic coating to the physico-mechanical behavior of a polypropylene substrate. Int J Adhes Adhes 2011;31:220–5.
[22] Kim W-S, Yun I-H, Lee J-J, Jung H-T. Evaluation of mechanical interlock effect on adhesion strength of polymer–metal interfaces using micro-patterned surface topography. Int J Adhes Adhes 2010;30:408–17.